Current Interrupt Technique to Fully Characterize PEMWE Cells

Journal of The Electrochemical Society, 2024 **171** 034509

Current Interrupt Technique to Fully Characterize PEMWE Cells

Tobias Krenz,[1,2,z] Torben Gottschalk,[2] Lennard Helmers,[1] Patrick Trinke,[2] Boris Bensmann,[2] and Richard Hanke-Rauschenbach[2]

[1]*Siemens Energy Global GmbH & Co. KG, 91058 Erlangen, Germany*
[2]*Leibniz University Hannover, Institute of Electric Power Systems, 30167 Hannover, Germany*

It is common practice to characterize cells in polymer electrolyte membrane water electrolysis (PEMWE) using electrochemical impedance spectroscopy (EIS) and Tafel analysis, which require special equipment and operation procedures. Additionally, these techniques are not suitable for large industrial size cells with very low impedances. We present a simpler approach based on a novel evaluation of the current interrupt (CI) technique. The CI technique utilizes the voltage response after an instantaneous drop of electric current to identify the ohmic resistance R_Ω, charge transfer resistance R_{ct} and double-layer capacity C_{dl} in a simplified equivalent circuit (EC) of the cell. A direct link to results of typical EIS and Tafel analysis can be defined by using the improved CI method which considers a non-linear activation resistance instead of a constant charge transfer resistance. Thereby, access to equivalent information as the established standard method is granted, while being applicable to all cell and stack sizes without requiring special equipment (e.g. impedance spectrometer). The agreement with experimental data is significantly improved over the assumption of a constant charge transfer coefficient. Consistency of the proposed interpretation with explicit EIS and Tafel analysis is demonstrated and options for industrial application of the evaluation scheme are discussed.
 [DOI: 10.1149/1945-7111/ad3057]

Manuscript submitted August 1, 2023; revised manuscript received January 23, 2024. Published March 18, 2024.

List of Symbol

α_a	anodic charge transfer coefficient	–
α_c	cathodic charge transfer coefficient	–
η_i	overpotential of component i	V
τ	time constant	s
F	faraday constant	96,485 C mol^{-1}
R	universal gas constant	8.314 J mol^{-1}
b_a	anodic Tafel slope	mV dec^{-1}
c	intercept with voltage axis for regression of η_{act} over log(t)	V
C_{dl}	capacitance of double layer	F cm^{-2}
i_0	exchange current density	A cm^{-2}
i_Ω	current density through membrane	A cm^{-2}
I_1	current density one sampling interval after CI	A cm^{-2}
i_{ct}	current density through charge transfer resistance	A cm^{-2}
I_{init}	current density before CI	A cm^{-2}
R_Ω	ohmic resistance	Ω cm
R_{ct}	charge transfer resistance	Ω cm
T_s	sampling interval	s
U_1	cell voltage one sampling interval after CI	V
U_{cell}	cell voltage	V
U_{init}	cell voltage before CI	V
U_{rev}	reversible cell voltage	V

The focus of this paper is the improvement of alternatives to standard cell characterization techniques in polymer electrolyte membrane water electrolysis (PEMWE) targeting simplification as well as application in an industrial environment.

PEMWE has been progressing toward one of the key technologies to produce green hydrogen.[1,2] Apart from cost, efficiency and degradation are still of concern.[3–6] Therefore, cell characterization is important to provide in situ information of a cell's state which allows to distinguish drivers for cell voltage increase. Repeated cell characterization over time allows to track changes in the contribution and therefore gain insights into degradation.[1]

In PEM lab cells, both for fuel cells and water electrolysis, a standard for in situ cell characterization has been established: electrochemical impedance spectroscopy (EIS) together with a Tafel analysis, which allows to quantify the parameters of a Tafel cell voltage model and contributions beyond.[7,8] The EIS measurements are performed, and a polarization curve is recorded. The first allows, among other characteristics to determine the ohmic resistance R_Ω, which is often done by using an quivalent circuit (EC) of a cell as can be seen in Refs. 9–11. After R_Ω has been measured, the polarization curve can be corrected for the ohmic overpotential. These reduced voltages are then used to perform a Tafel analysis to gain insights into the kinetics defining the rate determining reaction.[12]

However, this cannot be applied to large cells. For EIS the limitation lies in the maximum current that can be delivered. In Ref. 3 a limit of approximately 100 A is stated. Even if this limit was increased to 1000 A, for industrial size cells (e.g. 1 m^2 as stated in Ref. 13) this would give a maximum current density of 0.1 A cm^{-2}, which is too small to gain insights into typical operating ranges extending to 2 A cm^{-2}. In addition, the instruments are expensive and have limitations for industrial size cells with very low impedances, for high frequency measurements.[14] Hence, EIS is usually used in laboratories and not in commercial electrolysis stacks in the field.

Even if the ohmic resistance could be measured, a Tafel analysis can neither be performed. Longer operation periods at low current densities (e.g. several minutes with current densities ranging from 0.01 to 0.1 A cm^{-2}) as required to perform a Tafel analysis are typically not possible in industrial configurations, due to safety restrictions regarding foreign gas concentrations. This is due to increased volumetric hydrogen contents in oxygen on the anode side of the cell for small current densities.[15]

Other procedures for cell characterization are scarce. Sometimes only cell voltage and current density are used to determine parameters for describing a full polarization curve (e.g.[16,17]). However, they lack the comparison to the parameters obtained by EIS and Tafel analysis and focus solely on reproducing the net cell voltage.

One possibility is given by the so-called current interrupt method (CI): CI is a standard technique in electrochemistry and used in various systems to determine their ohmic resistance.[12] The current at

[z]E-mail: Tobias.Krenz@siemens-energy.com

which a system is operated is abruptly interrupted (or altered significantly) and from the instantaneous voltage response the ohmic resistance is determined.[12]

In PEM fuel cells (PEMFC) most publications consider CI as a technique to determine the ohmic resistance only (e.g.[8,18–20]). Other authors fit more complex equivalent circuits (ECs) to the measured response, as done in Refs. 21, 22. An interesting example is the work of Jaounen et al.[23,24] where it is shown that equivalent information as in the standard analysis can be gained by a single current interrupt event. Tafel slope, exchange current density, double layer capacity and proton conductivity of the membrane are calculated, and the results are compared with those obtained from EIS and Tafel analysis. Good agreement for current densities up to 0.2 A cm^{-2} is shown. In Refs. 23, 24 a slightly more complex polarization model is used for PEMFC than the one we are introducing in this work for PEMWE.

In PEMWE van der Merwe et al.[25] use CI with a Randles EC to determine R_Ω, R_{ct} and C_{dl}. The agreement with EIS measurements for R_Ω is good for the investigated current densities. For R_{ct} however, the agreement only holds for current densities of up to 0.1 A cm^{-2}. Martinson et al.[26] use a more complex EC that still consists of solely linear components. The procedure used to determine the EC's parameters is composed of four different steps that contain interruption of the current and stimulation of the system with a range of frequencies. However, this still does not allow to determine comparable information to the standard technique (e.g. Tafel slope and exchange current density remain unknown).

In contrast to these works, we introduce an improved, yet simple CI technique that allows to determine ohmic resistance, kinetic parameters of a Tafel model and the capacity of the double layer. Hence, equivalent insights as from the standard techniques is gained by a single interruption of the current and by steady state operation at a single low load point. We are using experimental data to directly compare results from standard cell characterization measurements (EIS & Tafel analysis) with dynamic voltage responses from CI measurements. The parameters R_Ω, C_{dl}, b_a, i_0 are derived with only small deviation from the values obtained by the aforementioned techniques.

The paper is structured as follows: First CI as a method for cell characterization is introduced by distinguishing between the interpretation of the immediate voltage response and the following voltage decay. The interpretation of the voltage decay requires considering the non-linearity of the charge transfer resistance. We are then introducing the experimental set up and the used protocols for cell conditioning, standard cell characterization and CI. This is followed by the results of standard cell characterization and cell characterization using CI including a comparison of both. Finally, we give an outlook and are concluding and summarizing our findings.

CI and Options for Interpretation

In this section two aspects of interpretation that can be applied to characterize a cell by CI are introduced. The immediate response, which is the standard utilization of the CI technique to determine the ohmic resistance of PEM cells, and the subsequent decay of the cell voltage. To analyze the decay, we present an improved evaluation, that includes the determination of the Tafel slope. To gain equivalent information as from EIS and Tafel analysis the evaluation of the cell voltage at a low current density, here 0.1 A cm^{-2} is used.

Immediate response.—A typical EC to describe a PEMWE cell's behavior is the simple Randles EC as used in Ref. 25, which is shown in Fig. 1.

In Fig. 1, R_Ω is the ohmic resistance, C_{dl} is the double layer capacitance and R_{ct} is the charge transfer resistance. The immediate voltage response is used to determine the ohmic resistance (cf. Fig. 2).

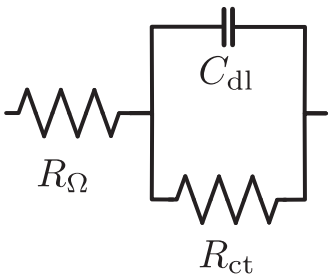

Figure 1. Randles equivalent circuit.

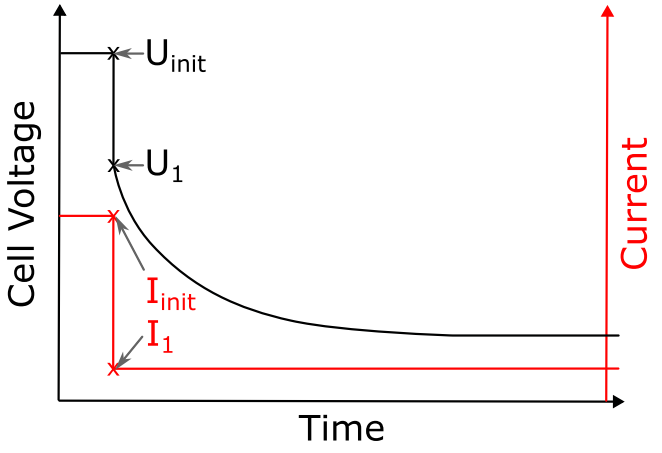

Figure 2. Schematic showing calculation of R_Ω using immediate voltage drop: voltage response (black) and electrolysis current (red).

When the current is interrupted the voltage over R_Ω disappears instantaneously. To calculate the ohmic resistance Eq. 1 is used:

$$R_\Omega = \frac{U_{init} - U_1}{I_{init} - I_1} \quad [1]$$

As long as the ohmic resistance is described by a single linear resistor connected in series with its neighboring components the calculation of the ohmic resistance remains unchanged even when more complex ECs are used.

Subsequent voltage decay.—The evaluation of the transient following the immediate voltage drop and the possibilities to determine R_{ct} (including Tafel parameters b_a and i_0), as well as C_{dl} is the focus of this work. Equation 2 together with Eq. 3 describe the discharge of a RC network with a constant charge transfer resistance and is introduced for the sake of comparison with the approach presented below.

$$\eta_{act}(t) = \eta^0_{act} \cdot e^{\frac{-t}{\tau}} \quad [2]$$

$$\tau = R_{ct} \cdot C_{dl} \quad [3]$$

When using the simple Randles EC with a constant R_{ct} parameterized by EIS, time constants for the discharge are typically in the range of double-digit milliseconds. According to Eqs. 2 and 3, after $5 \cdot \tau$ 99.3% of the activation overpotential should have vanished and the cell potential approaches Nernst potential. As shown in other publications (e.g.[23,25]) and in the results part of this work, this does not agree with the observed behavior in experiments, where the cell voltage approaches Nernst potential much slower. The experimental observation cannot be explained in this framework. Therefore, as prescribed by the polarization behavior, a non-linear charge transfer resistance whose resistance increases with decreasing current is used, which describes the slowed down discharge much more accurately.

Model equations.—The transient potential resulting from Randles EC, Eqs. 2 and 3, can be altered by allowing for non-constant resistance, R_{ct}. This is achieved by formulating the voltage over the charge transfer resistance using the Tafel equation:

$$\eta_{act} = b_a \cdot \ln\left(\frac{i_{ct}(t)}{i_0}\right) \quad [4]$$

By dividing Eq. 4 by the current passing R_{ct}, the effective resistance can be calculated:

$$R_{ct} = \frac{b_a \cdot \ln(i_{ct}(t)/i_0)}{i_{ct}(t)} \quad [5]$$

To fully describe the EC, Equations for an ideal capacitor (Eq. 6) and for Kirchhoff's current law (Eq. 7) are used.

$$C_{dl} \cdot \frac{d\eta_{act}(t)}{dt} = i_{dl}(t) \quad [6]$$

$$i_\Omega(t) - i_{ct}(t) - i_{dl}(t) = 0 \quad [7]$$

Manipulation of Eqs. 4, 6, and 7 gives:

$$\frac{d\eta_{act}}{dt} = \frac{i_\Omega(t)}{C_{dl}} - \frac{i_0}{C_{dl}} \cdot \exp\left(\frac{\eta_{act}(t)}{b_a}\right) \quad [8]$$

At times after a CI ($i_\Omega = 0$), Eq. 8 can be rewritten as:

$$d\eta_{act} \cdot \exp\left(-\frac{\eta_{act}}{b_a}\right) = -\frac{i_0}{C_{dl}} \cdot dt \quad [9]$$

Integration allows to solve the differential equation and further manipulation grants an explicit formulation of the voltage drop. This is given by Eq. 10 (cf. Appendix A.2 for the full mathematical derivation):

$$\eta_{act}(t) = -b_a \cdot \ln\left(t \cdot \frac{i_0}{b_a \cdot C_{dl}} + \frac{i_0}{I_{int}}\right) \quad [10]$$

Equation 10 is a slightly simplified version of the equation given in Ref. 23 and takes the differences between PEMFC and PEMWE into account, resulting in opposite signs. It describes the voltage discharge after the electrolysis current has reached 0 and contains only the activation overpotential. Equation 8 is more general than Eq. 10 and describes the activation overpotential during operation, ramping down, as well as after a shutdown.

Furthermore, it is important to note that the shown approach is not covering mass transport losses. To avoid any disturbance in the voltage decay caused by disappearing mass transport losses, a limited period after the current has been interrupted should be disregarded in the analysis or when using Eq. 8 only times with sufficiently low current densities should be considered. Guidance on how to choose a proper interval is given later in this section.

At voltages close to Nernst potential, the Tafel approximation may be replaced with the Butler-Volmer equation as detailed in Appendix A.1, but at times of the voltage response during which the cell potential is significantly above Nernst potential ($U_{cell} \geqslant 1.35\ V \gg U_{Nernst} \approx 1.19\ V$ is focus of this work, as shown in theExperimental setup section), the Tafel equation is a sufficiently accurate simplification (cf. Appendix A.1).

Parameter estimation.—To obtain R_{ct}, b_a, i_0, and C_{dl} a two step approach is proposed. In order to achieve good results the selection of an appropriate fit interval is important. Since mass transport losses are not covered by Eq. 10 the fit interval needs to be adjusted accordingly.

Firstly, the Tafel slope can be found from an η-vs-log(t) plot following Eq. 10. This is achieved by a linear regression of:

Figure 3. Experimental setup at Institute of Electric Power Systems.

$$y = -b_a \cdot \ln(t) + b_a \cdot \ln\left(\frac{b_a \cdot C_{dl}}{i_0}\right) \quad [11]$$

$$= -b_a \cdot \ln(t) + c \quad [12]$$

Equation 12 is only valid if the following inequality is kept $t \gg \frac{b_a \cdot C_{dl}}{I_{int}}$. A mathematical justification for Eq. 12 and the just mentioned criterion is given in Appendix A.3.

As in standard Tafel analysis, appearance of notable mass transfer losses is best to be avoided. To ensure this is maintained and mass transport losses have vanished, in the results part of this work, the interval used starts from 1 s after the current has been interrupted. The interval runs until the expected linear voltage vs log (t) relation is violated. The justification of this setting and further aspects of how to choose an appropriate interval are givenin the section about detailed discussion of discharge behavior.

After the Tafel slope and the parameter c have been determined, in a second step i_0 and C_{dl} can be derived. From Eq. 12 only the ratio $\frac{C_{dl}}{i_0}$ can be found, but considering a steady state measurement of the cell voltage allows to decouple i_0 and C_{dl}. The previously fitted value for b_a may be used and one additional steady state measurement at a low current density (in the following at 0.1 A cm^{-2}) is taken. At such a low current density the cell's overpotential consist predominantly of ohmic and activation losses and residual losses can be neglected. Both values are then used to evaluate Eq. 4 and solve for i_0:

$$i_0 = i \cdot \exp\left(\frac{\eta_{act}(i)}{b_a}\right) \quad [13]$$

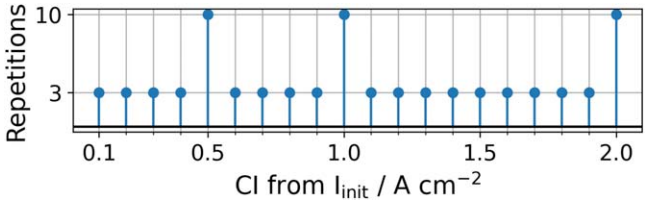

Figure 4. CI experiment: operating ranges and repetitions.

$$= i \cdot \exp\left(\frac{U_{\text{cell}} - U_{\text{rev}} - i \cdot R_{\Omega}}{b_{\text{a}}}\right) \quad [14]$$

This allows to fully decouple i_0 and C_{dl} by linking the transient response with steady state data.

Finally, C_{dl} can be calculated using Eqs. 11 and 12 which gives:

$$C_{\text{dl}} = \frac{b_a}{i_0} \cdot \exp\left(\frac{c}{b_a}\right) \quad [15]$$

For sampling intervals much longer than the reported $5 - 10$ ns[27,28] the measured voltage response can be corrected by the contribution of the voltage drop due to the intermediate discharge of the double layer, provided that b_a, i_0 and C_{dl} are known and the current is interrupted instantaneously.

$$R_{\Omega}^{\text{corrected}} = \frac{U_{\text{init}} - U_1 - \Delta\eta_{\text{act}}(\delta t)}{I_{\text{int}} - I_1} \quad [16]$$

$$\Delta\eta_{\text{act}}(\delta t) = -b_a \cdot \ln\left(\frac{I_{\text{int}}}{i_0}\right) + b_a \cdot \ln\left(\delta t \cdot \frac{i_0}{b_a \cdot C_{\text{dl}}} + \frac{I_{\text{int}}}{i_0}\right) \quad [17]$$

The intermediate discharge is calculated using Eq. 17, which is used to calculate the discharge corrected value of R_{Ω} in Eq. 16. The discharge interval δt can be set to half the sampling interval:

$$\delta t = 1/2 \cdot T_{\text{s}} \quad [18]$$

In general, EIS and CI methods do not produce the same results and some deviation is to be expected. For PEMFCs, where the use of CI for cell characterization seems to be more common than for PEMWE, the preferred technique for assessing a cell's ohmic resistance varies for different individual research groups.[19]

Experimental Setup

In the following, the experimental setup and the used test protocols are described.

Hardware setup.—A 4 cm^2 single PEM water electrolysis cell (Fraunhofer Institut für Solare Energiesysteme) is used for the CI measurements.[29] The cell contains a catalyst coated membrane (CCM) with Nafion N115. The anode is coated with 2.0 mg cm^2 Ir as a catalyst and the cathode with 1.0 mg cm^2 Pt. On the anode side a 1.0 mm titanium porous transport layer (PTL) and a 214 μm hydrophobic graphite PTL (Freudenberg, E20H) on the cathode side is used. The experiments are performed at a test bench which is shown in Fig. 3.

All measurements are executed at a cell temperature of 80 °C, ambient pressure and an anode water feed of 100 mL mim^{-1}. A Biologic SP-150 potentiostat with a 20 A booster is used to perform the CI and impedance measurements.

Test protocol.—To assure stable performance of the samples, the cell is conditioned for 1 h at 80 °C. This is followed by the measurement of three polarization curves with integrated impedance measurements (POL-EIS-curve) in a current density range of $0.001 - 4$ A cm^{-2}. Each current density is held for 20 s with a subsequent galvanostatic impedance measurement in the frequency ranges from 1 Hz to 100 kHz and an amplitude of 10% of the current value.

The CI measurements are repeatedly performed at different current densities which is visualized in Fig. 4. The current density I_{int} at which the cell is operated before the CI, ranges from 0.1 to 2.0 A cm^{-2}. The current is then interrupted by setting the current to 0 A. This is done using the CI program provided by the potentiostat. This allows to analyze the method over a wide range of operation. In total 81 CI measurements are performed for various initial current densities I_{int}: three repetitions at each 0.1 A cm^{-2}-step except for current densities of 0.5, 1.0 and 2.0 A cm^{-2} for which 10 repetitive measurements are performed (cf. Fig. 4).

Before every CI measurement the current I_{int} is kept constant for 5 min to stabilize the cell with a data acquisition time of 100 ms. Following this the current is interrupted for 10 s and the cell voltage is recorded every 0.2 ms. To ensure that the cell does not switch into fuel cell mode and to prevent any unwanted changes in the catalysts a minimum cell potential is set at 1.3 V. If the cell voltage reaches this threshold the protocol proceeds to the next stabilization step. It turned out that the voltage threshold is not reached in any of the CIs performed.

After the CI experiments are completed the POL-EIS curve measurements (as performed before the CI experiment) are repeated to assess the stability of the electrolysis cell after the CI measurements. This allows to compare the BoT and EoT state of the cell.

Results

Firstly, for the sake of comparison the cell characteristics obtained using standard cell characterization techniques (EIS and Tafel analysis) are shown. This is followed by the results of the CI analysis. Finally, a comparison of the CI results with the standard characterization technique is given.

Standard cell characterization methods.—The results of established standard characterization by EIS and Tafel analysis are summarized in Table I. Further details are available in Appendix B. The variation of cell characteristics before/after the CI experiments turn out to be very limited. The high repeatability of standard characterization results assures a good basis for comparison of characterization methods. An average of recordings before and after CI experiments is used for comparison with CI-based results.

Current interrupt.—In the following, the results obtained from CIs from 2.0Acm^{-2} are shown. The calculation of the ohmic resistance and the subsequent voltage decay are typically decoupled. The focus of this work is on describing the subsequent decay. This section is closed with results for the ohmic resistance corrected by the intermediate discharge. This is relevant since we are using a rather scarce sampling interval of 0.2 ms.

Table I. Cell characterization using EIS and Tafel analysis including reproducibility of the measurements (1σ). The ohmic resistance R_{Ω} is obtained using the mean HFR for current densities ranging from 0.3 to 2.0 A cm^{-2} and the double layer capacity C_{dl} for a current density of 2.0 A cm^{-2}.

	R_{Ω} in mΩ cm^2	b_{a} in mV dec^{-1}	i_0 in A cm^{-2}	C_{dl} in mF cm^{-2}
BoT	126.5 ± 0.02%	43.10 ± 0.37%	$1.04e-7 \pm 5.2\%$	62.48 ± 0.18%
EoT	126.0 ± 0.03%	43.18 ± 0.36%	$9.48e-8 \pm 3.6\%$	61.67 ± 0.63%
Combined/ Average	126.2 ± 0.21%	43.14 ± 0.38%	$9.94e-8 \pm 6.6\%$	62.08 ± 0.66%

Table II. Cell characterization using CI from I_{init} = 2.0 A cm^{-2} including reproducibility (1σ).

R_Ω in mΩ cm^2	$R_\Omega^{corrected}$ in mΩ cm^2	b_a in mV dec^{-1}	i_0 A cm^{-2}	C_{dl} in mF cm^{-2}
131.3 ± 0.07%	129.34 ± 0.07%	42.45 ± 0.76%	8.21e − 8 ± 10.5%	53.85 ± 1.85%

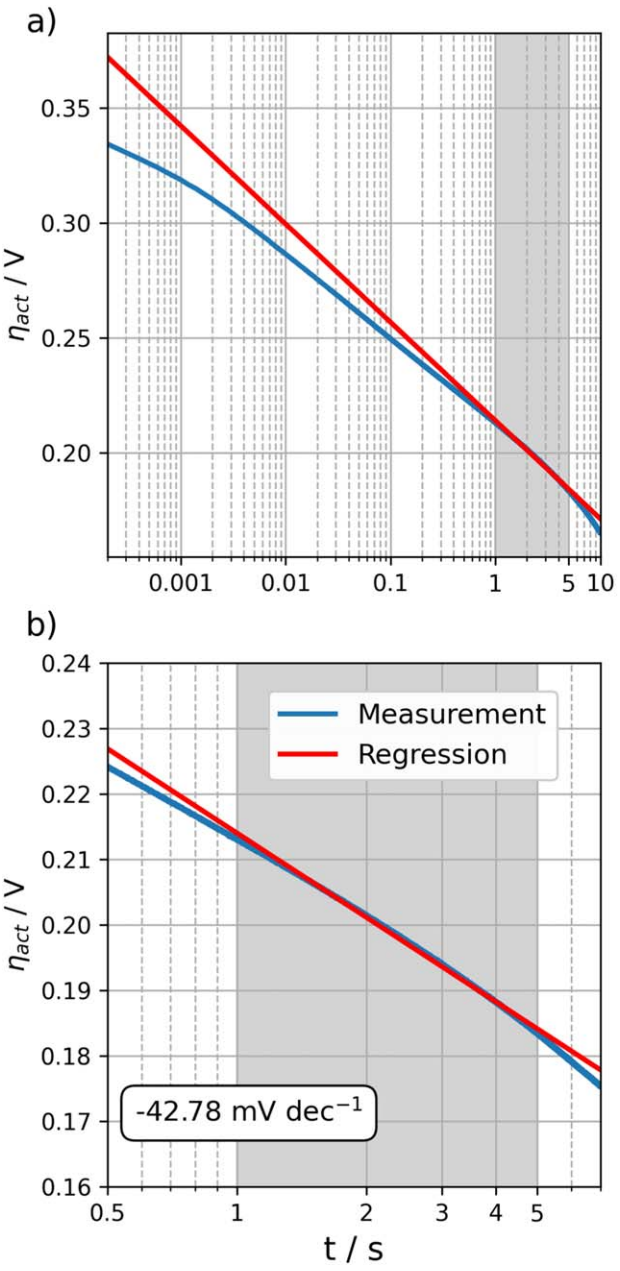

Figure 5. Regression in time domain for CI from 2.0 A cm^{-2}: measured discharge (blue) and regression (red).

Instant drop.—The results for the ohmic resistance R_Ω determined for CIs from $I_0 = 2.0$ A cm^{-2} are shown in Table II. The obtained values are on average 3.9% larger than those from the EIS measurements. The ohmic resistance can be corrected for the time passing between voltage recordings. This requires the knowledge of the parameters b_a, i_0, and C_{dl}. Details are discussed at the end of the section on the comparison of results. It can be assumed that this deviation can be reduced with shorter sampling intervals.[27]

Subsequent voltage decay.—Applying the scheme presented in CI and options for interpretation section for Eq. 10, a linear regression over log(t) can be performed which is shown in Fig. 5. In a second step, the resulting Tafel slope is used to determine i_0 and C_{dl} by an evaluation of the cell voltage at a steady load point of 0.1 A cm^{-2}.

Comparison of results.—In the following, the cell characteristics determined using standard and the proposed methods are compared.

Ohmic resistance.—Two values for the ohmic resistance calculated using CI are given: The direct response without and with the correction for the discharge that has happened (cf. Eqs. 17, 16). The values are compared with EIS results. The correction can only be calculated if the parameters b_a, i_0, and C_{dl} are known.

Both values are in good agreement with the HFR that is measured using EIS over the entire range invesitaged current densities. However, an offset of 5.5% with respect to the mean HFR measurements can be observed for the direct CI method. When applying the previously introduced correction (cf. Eqs. 16) the offset can be reduced to 3.9%. We thus assume that shorter sampling intervals would reduce the deviation. This is in agreement with the findings in Refs. 27 and 30. Other suggestions on how to improve the agreement are given in the section on possible improvements.

In Fig. 6a the results of the calculation of the ohmic resistance are shown for all 81 CI measurements where blue dots show the direct calculation, green dots the discharge corrected values, and red dots the values obtained using EIS. The measurement of the latter is further described in Appendix B.

As can be seen in Fig. 6a the agreement remains very good over the entire range from which the CIs are executed. Moreover, all methods show similar trends. For current densities below 0.3 A cm^{-2} the ohmic resistance is significantly lower than for current densities above 0.3 A cm^{-2} and for current densities above, the ohmic resistance reaches a plateau. The increase of the ohmic resistance before the plateau however, is shifted by around 0.1 A cm^{-2} toward smaller current densities when using CI instead of HFR measurements.

Multiple measurements are barely visible in Fig. 6a, indicating the good reproducibility of results.

Tafel parameters.—The calculation of the Tafel slope is performed by fitting the voltage decay as described by Eq. 12. In a subsequent step the exchange current density is calculated using an additional evaluation of a single steady state load point at 0.1 A cm^{-2} to solve Eq. 13.

In Fig. 6b the results obtained from CI measurements from various initial current densities are shown (blue dots). These are compared with the results obtained from standard cell characterization (black line, gray face showing standard deviation, for more details see Appendix B). For all current densities a good agreement is shown. However, for initial current densities smaller than 0.3 A cm^{-2}, the values obtained from CI tend to be slightly lower than the reference. From 0.6 A cm^{-2} upward the calculated Tafel slope slowly approaches the values measured using the standard technique (43.14 mV dec^{-1}) and remain stable for larger values of the initial current I_{int}.

In Fig. 6c the fitted exchange current density is compared with the measured one using EIS and Tafel analysis. The blue dots are obtained using the calculated Tafel slope and an additional evaluation of a steady state voltage at $i = 0.1$ A cm^{-2}. The black line shows

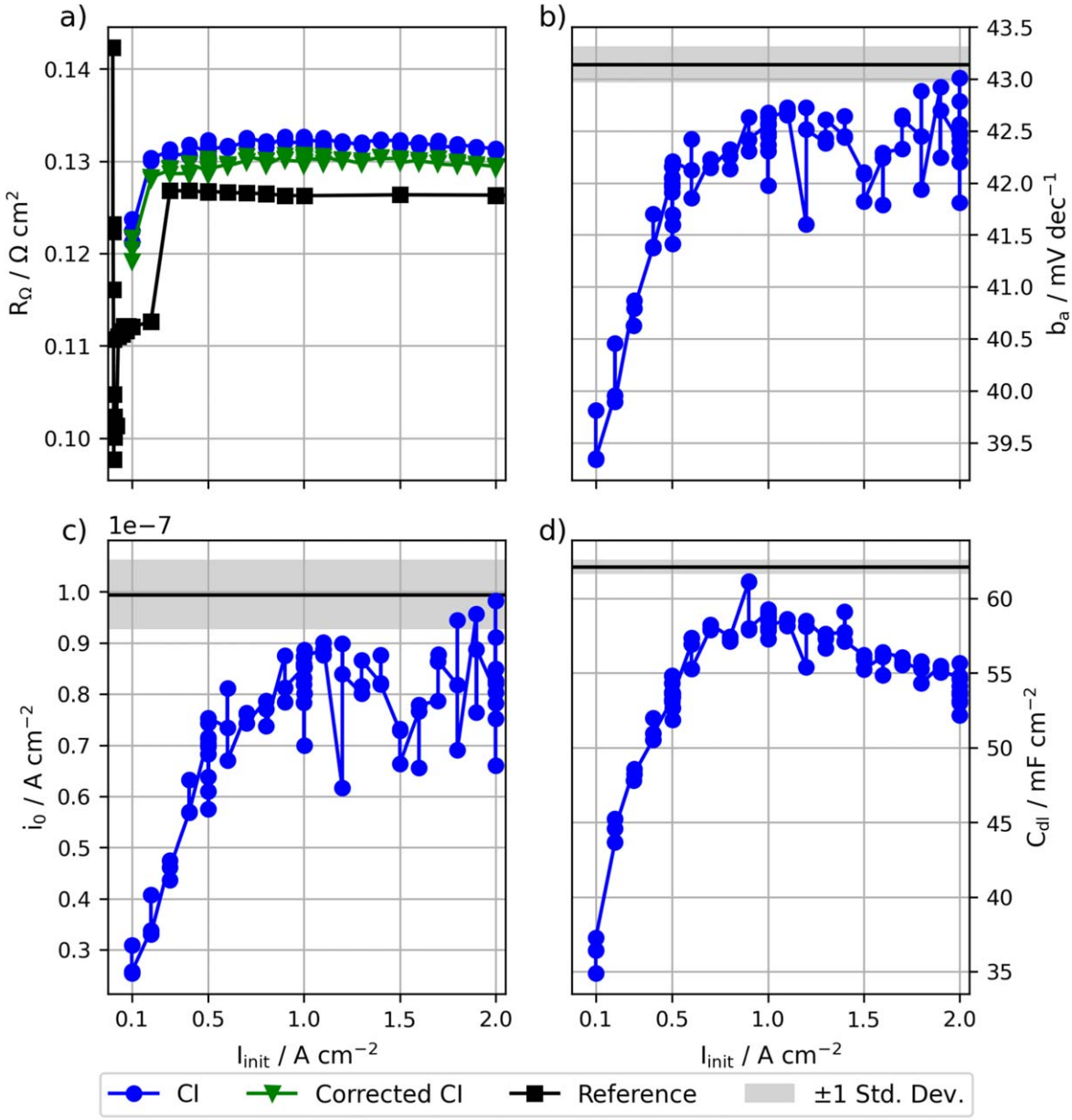

Figure 6. Cell characteristics obtained using EIS and Tafel analysis (black line/squares, gray face showing one standard deviation) compared with CI (blue line/dots): (a) ohmic resistance (green line/triangles showing discharge corrected values for ohmic resistance obtained using CI), (b) Tafel slope, (c) Exchange current density, (d) double layer capacity (reference obtained using EIS at 2 A cm^{-2}).

the measured exchange current density using the standard Tafel analysis and the gray face the corresponding standard deviation. The values obtained from CI are systematically smaller which is due to the deviation in the obtained Tafel slope. However, the deviations are rather small, especially for larger values of I_{int}.

Double layer capacity.—The double layer capacity is calculated using the previously obtained values for the Tafel slope and exchange current density which allow to solve Eq. 15. A comparison of the resulting values using EIS at a current density of $i = 2.0$ A cm^{-2} and CI is given in Table II for $I_{\text{int}} = 2.0$ A cm^{-2} and in Fig. 6d for various values of I_{int}. The values calculated using CI are slightly smaller than the one using EIS. Both deviations for i_0 and C_{dl} follow a similar trend, which is related to the coupling as expressed in Eq. 12.

Discharge correction.—The discharge correction can only be performed after the cell has been fully characterized. Assuming an ideal step-wise current interrupt, the voltage can be expected to drop in the interval between two recordings as prescribed by the exponential voltage decay.

For the used sampling interval of $T_s = 0.2$ ms, $I_{\text{int}} = 2.0$ A cm^{-2} and the parameters from Table II, together with Eqs. 16 and 17 this leads to:

$$\Delta\eta_{\text{act}}(\delta t = T_s/2,\ I_{\text{int}} = 2\ \text{A cm}^{-2}) = 3.38\ \text{mV} \quad [19]$$

$$\Delta R_\Omega = \frac{\Delta\eta_{\text{act}}}{I_{\text{int}} - I_{\text{l}}} = 1.91\ \text{m}\Omega\ \text{A cm}^2 \quad [20]$$

$$R_\Omega^{\text{corrected}} = 129.34\ \text{m}\Omega\ \text{cm}^2 \quad [21]$$

This reduces the offset of the calculated ohmic resistance for $I_{\text{init}} = 2.0$ A cm^{-2} from 3.9% to 2.4%. For the entire range of current densities investigated, the discharge correction improves

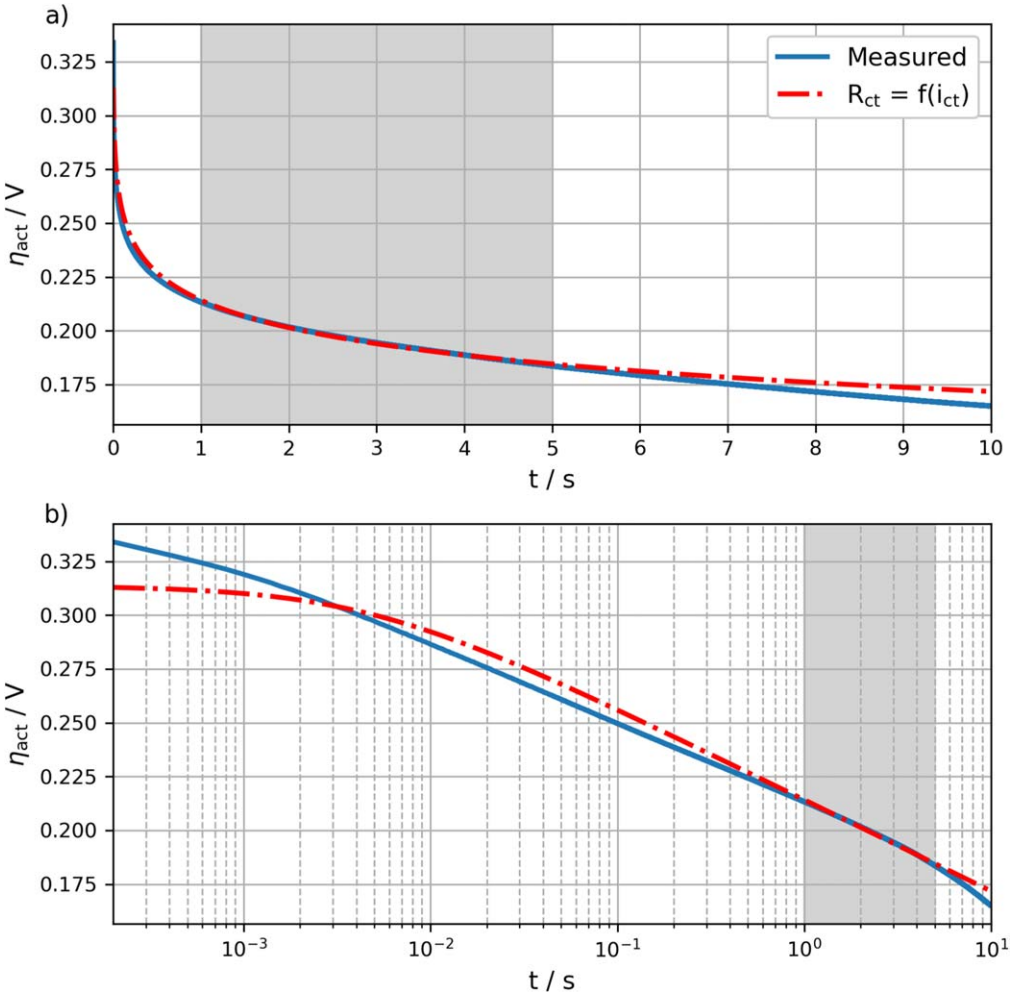

Figure 7. Discharge behavior for CI from 2.0 A cm^{-2}: measured (solid blue line), using a Randles EC with non-linear R_{ct} (dash-dotted red line) and used fit interval (gray face).

the agreement between EIS and CI significantly (cf. Fig. 6a). Over the investigated range the mean offset of 5.5% is reduced to 3.9%.

Discussion

The following section discusses the discharge behavior and gives a justification of the chosen fit interval. Moreover, requirements, limitations and possible improvements of the proposed approach are given.

Detailed discussion of discharge behavior.—The discharge behavior after the immediate voltage response is shown in Fig. 7 where the measurement is given by the solid blue line, the simulated discharge based on Eq. 10 with parameters from Table II by the red dash-dotted line and the fit interval by the gray face.

Since mass transport losses are not part of the presented approach they have to be considered when choosing a start time of the fit interval. The stop time of the fit interval is chosen by considering the expected linearity of the discharge over $log(t)$. As shown in Fig. 7b during the first 2 ms of the voltage decay, the cell voltage remains above the calculated values.

This offset could be explained by mass transport losses. However, longer time constants for the mass transport losses are reported in Ref. 31 with $\tau = 0.1$ s. The disappearing mass transport losses might also be overlapped by the cathodic discharge which is supposed to be much faster than the anodic discharge whilst being much smaller in magnitude. In an EC containing RC circuits for both anode and cathode side the immediate discharge of the cathodic double layer would likely to dominate the voltage response within the first milliseconds. Apart from the disappearing mass transport losses this might be the dominate cause for deviations between simulation and measurement during this interval.

Other than avoiding disappearing mass transport losses, when using the presented approach for cell characterization, it is important to maintain the criterion defined by Eq. 12. This is necessary since the Tafel slope was calculated using a linear regression over a logarithmic time axis. As can be seen in the measured discharge in Fig. 7b this linearity is reached after around 0.1 s after the current has been interrupted. For smaller values of I_{int} this time increases, which is why we have chosen 1.0 s in order to achieve good results for varying current densities without using adaptive intervals.

The end time of the fit interval was set to 5 s after the current was interrupted which is due to the accelerated discharge that can be seen in Fig. 7b. This accelerated voltage drop can be explained by a change in the Nernst potential. After a longer period without electrolysis current, the concentration of product gases in the cell decreases causing a decreasing of the Nernst potential.[32] However, such a correction is not included in our calculations. Another explanation for the accelerated discharge can be found by considering the discharge current (cf. Fig. 8) for times of the accelerated discharge and linking them with Tafel analysis in Fig. B·3. In the Tafel analysis given in Fig. B·3, the observed slope tends to increase for such small current densities, which would explain an increased discharge rate for times when the discharge current falls below a certain value.

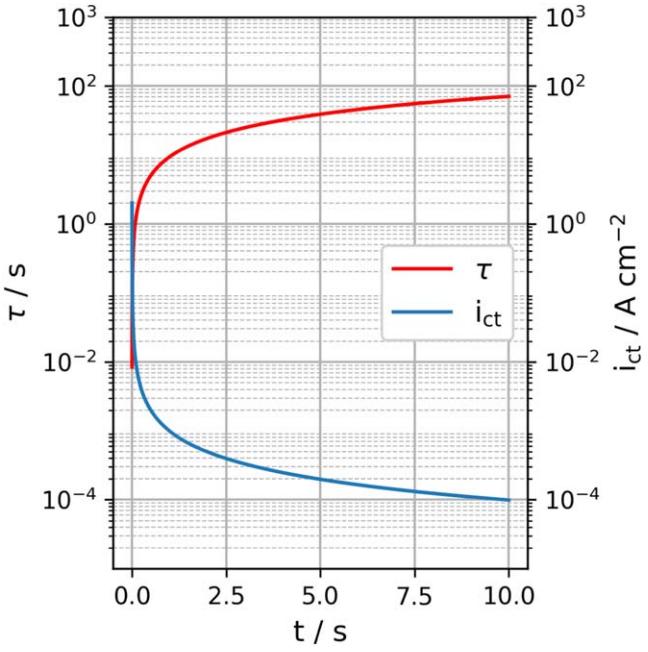

Figure 8. Time constant $\tau_{ct}(t) = R_{ct}(i_{ct}(t))\cdot C_{dl}$ (red) and current $i_{ct}(t)$ (blue) of double layer discharge for CI performed from 2.0 A cm^{-2}.

CI's demands for cell characterization.—CI for cell characterization has certain demands on the available sampling intervals of the sensor data, the ramp rate as well as the maximum current at which a cell can be operated.

Sampling intervals.—The high demands for sampling intervals of 5 – 10 ns that are formulated for CI in literature (e.g.[27,28]) do not seem entirely necessary. This demand is only formulated for the calculation of the ohmic resistance. However, even for the provided 0.2 ms the results aligned well with EIS measurements and could even be improved by considering the voltage drop due to the intermediate discharge of the double layer between two voltage measurements.

The calculation of the kinetic parameters should not require sampling intervals shorter than 100 ms. This becomes obvious when looking at the time constant of the discharge obtained by the improved CI method (cf. Fig. 8). Even for cells with very low activation overpotential and very small double layer capacity the suggested 100 ms are still sufficient. The minimum requirements for the sampling rate of the sensors can be reduced drastically, especially when focusing on the Tafel parameters.

Ramp rate and maximum remaining current.—Minimum requirements for the ramp rate for the current profile during shutdown/interrupt and the maximum remaining current after the current has been cut (cf. I_1 in Fig. 2) still need to be determined. Both points need to be discussed when applying this method to industrial scale cells or stacks. In industrial applications the power electronics are likely to be significantly slower in interrupting the electrolysis current than laboratory equipment.

In Fig. 8, a minimum current can be derived by analyzing the corresponding time constant. In order to reduce the time constant to values above 1 s the discharge current needs to fall below 0.01 A cm^{-2}.

Repeatedly switching a PEMWE cell off and on can increase the cells degradation compared to more steady operation.[33] This effect can be significantly reduced when, instead of switching to open circuit voltage a certain cell potential (e.g. 1.3 V) is maintained.[34] As shown in the result part of this work, the activation overpotential remains above 0.15 V for the full 10 s the current is interrupted and therefore the cell potential remains well above 1.3 V, leaving sufficient time for analyzing the voltage decay.

Similarities with Tafel equation.—The similarities of Eq. 10 and Eq. 4 (Tafel equation) are obvious. In the following a short interpretation of the parameters in Eq. 10 is given.

Since the equation is only valid as long as the voltage remains positive the corresponding criterion is formulated in Eq. 22:

$$t \leqslant t_{max} = \frac{I_{int} - i_0}{I_{int}\cdot i_0}\cdot b_a \cdot C_{dl} \qquad [22]$$

For an initial current of $I_{int} = 2.0$ A cm^{-2} and the corresponding parameters from Table II this gives $t_{max} = 1.45 \times 10^4$ s. Analogously to i_0 for the Tafel equation, t_{max} marks the value where the activation potential switches signs. Anything in close proximity to this value is therefore not well described by Eq. 10. As can be seen in the results part of this work, the discharge leaves the predicted decay much earlier (after around 5 to 6 s) and the cell voltage begins to decrease faster. As discussed in the Detailed discussion of discharge behavior section this could be due to a change in the Nernst potential or the observed higher Tafel slope for very small current densities in Appendix B.

Possible improvements.—In the following, possible improvements regarding the presented method are discussed.

Reducing the offset in calculated ohmic resistances.—As shown in Fig. 6a the values for R_Ω obtained from CI are systematically larger than the values generate using EIS measurements. Two possible phenomena might help to further explain the remaining deviations:

(i) Distinguishing between anodic and cathodic activation overpotential (η^a_{act} and η^c_{act}) changes the predicated discharge in-between two voltage measurements as described in Eq. 16. Due to a higher reaction rate on the cathode (compared to the anode) the time constant of the cathodic discharge is much smaller than the time constant of the anodic discharge ($\tau^a_{act} \gg \tau^c_{act}$). However, it is important to point out that the anodic overpotential is much larger than the cathodic overpotential.

(ii) Considering the voltage drop due to disappearing mass transport losses.As pointed out in the CI and options for interpretation section the presented approach does not cover mass transport losses. Hence, a voltage during the time step in which the current is interrupted caused by decreasing mass transport losses is not captured and might interfere with the calculation of R_Ω. However, this effect only a has small contribution. The reduction of η_{mt} after the current is interrupted can be described as follows:

$$\Delta\eta_{mt}(t) = \Delta\eta^0_{mt}\cdot(1 - \exp(-t/\tau_{mt})) \qquad [23]$$

For $\eta^0_{mt} = 5$ mV for $i = 2.0$ A cm^{-2} and an assumed time constant of $\tau_{mt} = 100$ ms[31] this gives:

$$\Delta\eta_{mt}(t = 0.2\text{ ms}) = 0.1\text{ mV} \qquad [24]$$

which leads to a neglectable correction of R_Ω of:

$$\Delta R_{\Omega,mt} = \frac{\Delta\eta_{mt}(t = 0.2\text{ ms})}{I_o - I_1} = 0.056\ \text{m}\Omega\,\text{cm}^2 \qquad [25]$$

Simultaneous fitting.—Simultaneously fitting the steady state data and voltage decay should allow to better estimate the parameters. The steady state polarization curve is given by:

$$U_{\text{cell}}(i) = U_{\text{rev}} + i \cdot R_{\Omega}(i) + b_{\text{a}} \cdot \ln(i/i_0) + \eta_{\text{mt}}(i) \quad [26]$$

Additionally, when applying this coupled approach containing the steady state polarization, time-dependent currents, I_{int}, and respective implicit mass transport losses can be accounted for. Aside from that, the sensitivity to random noise of measurement signals should reduced if data from a longer recording interval is accounted for.

Summary, Conclusion, and Outlook

Using a revised interpretation performed for current densities ranging from 0.1 to 2.0 A cm^{-2} a full cell characterization including ohmic resistance, Tafel parameters, double layer capacitance and an assessment for mass transport overpotentials can be obtained at comparable quality to standard characterization using EIS and Tafel measurements.

Regarding the ohmic resistance, the deviations between EIS and CI for sampling intervals of 0.2 ms are rather small (3.9% for measurements performed from 2.0 A cm^{-2}). A reduction to deviations of 2.4% can be achieved by considering the discharge that is taking place in between the two initial voltage measurements.

When considering the non-linearity of the charge transfer resistance, the Tafel slope can be calculated. For a reliable calculation of exchange current density and capacity of the double layer an additional evaluation of the cell voltage at one steady load point of 0.1 A cm^{-2} is used. A short operation of 60 s at a relatively small current density seems feasible with respect to foreign gas concentrations. Deviations between standard procedure (EIS and Tafel analysis) are small for all current densities at which the CI was performed. Demands on sampling rate are only high for the calculation of the ohmic resistance and can be relaxed using methods proposed in the Discussion section. For the calculation of b_a, i_0 and C_{dl} they lie in the range of 1 s.

Additionally, the agreement of the measured and the predicted voltage response is significantly improved by considering the non-linearity of charge transfer resistance. It exceeds the advances reported in literature through more complex ECs. This good agreement remains for the full 10 s the current is interrupted.

It is also important to point out, that even though the fit interval needs to be adjusted two criteria for the selection of an appropriate fit interval could be formulated leaving sufficient data for meaningful evaluation. The first is to rule out significant disturbances caused by disappearing mass transport losses. The second is the linearity of the discharge over $\log(t)$.

Results indicate that a cell characterization that gains equivalent insights as EIS and Tafel analysis can be performed without the limitations of the standard techniques with regards to cell size and smallest applicable load (in regards to foreign gas concentrations). Hence, we believe it helps to understand degradation processes in industrial scale cells and allow to monitor the state of a cell/stack in industrial applications.

In future work we will further refine requirements on sampling and ramp rate as well as the maximum current after a CI. Additionally, we plan to introduce CI measurements in degradation tests to assess the long-term sensitivity of our approach. Since the technique can be applied to industrial scale cells and stacks experiments and data analysis are planned accordingly.

Appendix A. Model Equations: Derivations and Alternative Formulations

In this section alternative formulations, the mathematical derivation and justifications for the equations used in this work are shown.

A.1. Model equations using butler volmer.—Instead of using the Tafel equation to calculate the activation overpotential one could use the Butler-Volmer equation:[35]

$$i_{\text{ct}} = i_0 \cdot \left\{ \exp\left(\frac{2 \cdot \alpha_{\text{a}} \cdot \text{F}}{\text{R} \cdot T} \cdot \eta_{\text{act}} \right) - \exp\left(-\frac{2 \cdot \alpha_c \cdot \text{F}}{\text{R} \cdot T} \cdot \eta_{\text{act}} \right) \right\} \quad [A\cdot1]$$

Together with Eqs. 6, 7 and further manipulation this yields:

$$\frac{d\eta_{\text{act}}}{dt} = \frac{i_{\Omega}(t)}{C_{\text{dl}}} - \frac{i_0}{C_{\text{dl}}} \cdot \left\{ \exp\left(\frac{2 \cdot \alpha_{\text{a}} \cdot \text{F}}{\text{R} \cdot T} \cdot \eta_{\text{act}} \right) - \exp\left(-\frac{2 \cdot \alpha_c \cdot \text{F}}{\text{R} \cdot T} \cdot \eta_{\text{act}} \right) \right\} \quad [A\cdot2]$$

However, in the experimental data used in this work the cell voltage remains above 1.35 V which is the equivalent of an activation overpotential of around 0.16 V. For symmetric charge transfer coefficients ($\alpha_a = \alpha_c = 0.5$) and an operating temperature of 80 °C this yields:

$$i_{\text{ct}} = i_0 \cdot \{\exp(5.26) - \exp(-5.26)\} \quad [A\cdot3]$$

The contribution of the backward reaction is not significant for such cell potentials, hence, the Tafel equation a valid simplification of the Butler-Volmer equation. This statement also holds for $\alpha_a > \alpha_c$. For example, for $\alpha_a = 0.9$ and $\alpha_c = 0.1$:

$$i_{\text{ct}} = i_0 \cdot \{\exp(9.46) - \exp(-1.05)\} \quad [A\cdot4]$$

A.2. Derivation of explicit discharge equation.—In the following the detailed manipulations for the formulation of Eq. 10 are presented.

Firstly, Eq. 9 is integrated:

$$\int_{\eta_{\text{act}}(t=0)}^{\eta_{\text{act}}(t)} \exp\left(-\frac{\eta_{\text{act}}}{b_a} \right) d\eta_{\text{act}} = \int_{t=0}^{t} -\frac{i_0}{C_{\text{dl}}}\, dt \quad [A\cdot5]$$

Which gives:

$$\left[-b_a \cdot \exp\left(-\frac{\eta_{\text{act}}}{b_a} \right) \right]_{\eta_{\text{act}}(t=0)}^{\eta_{\text{act}}(t)} = \left[-\frac{i_0}{C_{\text{dl}}} \cdot t \right]_{t=0}^{t} \quad [A\cdot6]$$

The activation overpotential at $t_0 = 0$ can be calculated with $I_{\text{int}} = i(t_0)$ and $\eta_{\text{act}}(t_0) = b_a \cdot \ln(\frac{I_{\text{int}}}{i_0})$. Using these integration limits yields:

$$-b_a \cdot \exp\left(-\frac{\eta_{\text{act}}(t)}{b_a} \right) + b_a \cdot \exp\left(-\ln(I_{\text{int}}/i_0)\right) = -\frac{i_0}{C_{\text{dl}}} \cdot t \quad [A\cdot7]$$

Rearranging gives:

$$\exp\left(-\frac{\eta_{\text{act}}(t)}{b_a} \right) = \frac{i_0}{b_a \cdot C_{\text{dl}}} \cdot t + \frac{i_0}{I_{\text{int}}} \quad [A\cdot8]$$

Which finally leads to the explicit formulation given by Eq. 10:

$$\eta_{\text{act}}(t) = -b_a \cdot \ln\left(\frac{i_0}{b_a \cdot C_{dl}} \cdot t + \frac{i_0}{I_{\text{int}}} \right)$$

This explicit formulation of the activation overpotential also allows to formulate the discharge current explicitly:

$$\eta_{\text{act}}(t) = \eta_{\text{act}}(i_{\text{ct}}(t)) \quad [A\cdot9]$$

$$-b_a \cdot \ln\left(\frac{i_0}{b_a \cdot C_{dl}} \cdot t + \frac{i_0}{I_{\text{int}}} \right) = b_a \cdot \ln\left(\frac{i_{\text{ct}}(t)}{i_0} \right) \quad [A\cdot10]$$

$$i_{ct}(t) = \frac{b_a \cdot C_{dl} \cdot I_{init}}{t \cdot I_{init} + b_a \cdot C_{dl}} \quad [A\cdot11]$$

A.3. Derivation of equation used for linear regression.—We start to solve Eq. 12 for $log(t)$ by manipulating Eq. 10:

$$\ln\left(\exp\left(\frac{-\eta_{act}(t)}{b_a}\right) - \frac{i_0}{I_{init}}\right) = \ln(t) - \ln\left(b_a \cdot \frac{C_{dl}}{i_0}\right) \quad [A\cdot12]$$

Further manipulation yields:

$$\frac{-\eta_{act}}{b_a} + \ln\left(1 - \exp\left(\frac{\eta_{act}(t)}{b_a}\right) \cdot \frac{i_0}{I_{init}}\right) = \ln(t) - \ln\left(b_a \cdot \frac{C_{dl}}{i_0}\right) \quad [A\cdot13]$$

Which finally gives:

$$\eta_{act}(\ln(t)) = -b_a \cdot \ln(t) + b_a \cdot \ln\left(b_a \cdot \frac{C_{dl}}{i_0}\right) + b_a \cdot \ln\left(1 - \exp\left(\frac{\eta_{act}(t)}{b_a}\right) \cdot \frac{i_0}{I_{init}}\right) \quad [A\cdot14]$$

This can be approximated by Eq. 12 which is valid when $\frac{i_0}{b_a \cdot C_{dl}} \cdot t \gg \frac{i_0}{I_{init}}$ which gives:

$$t_{min} \gg \frac{b_a \cdot C_{dl}}{I_{init}} \quad [A\cdot15]$$

For the measured parameters in th section on standard cell characterization methods this gives for $t_{min}(I_{init} = 2.0\ A\ cm^{-2}) = 0.6$ ms and for $t_{min}(I_{init} = 0.1\ A\ cm^{-2}) = 12.5$ ms. In order to perform the simple regression as introduced in the section on Current interrupt the fit interval should start at least one order of magnitude after these calculated values. Since we have chosen the fit interval to start at 1.0 s this condition is kept for all the results shown in this work. It still allows a decent interval of 4 s duration for relevant data collection.

Appendix B. Standard Cell Characterization

In the following the results for the standard cell characterization consisting of EIS and Tafel analysis are presented.

B.1. Electrochemical impedance spectroscopy.—Figure B·1 shows the measured impedances in a Nyquist plot for 5 chosen current densities varying from 0.3 to 2.0 A cm^{-2}. These impedances are analyzed using Randles EC which is shown in Fig. 1. The time constant τ can be calculated by

$$\tau = \frac{1}{2 \cdot \pi \cdot f_0} \quad [B\cdot1]$$

where f_0 is the frequency in Hz for which $Im(-Z)$ reaches its maximum value.[11] For 2.0 A cm^{-2} a double layer capacity of 62.5 mF cm^{-2} is calculated. In Fig. B·2 the measured high frequency resistance (HFR) is shown for current densities between 0.001 and 4.0 A cm^{-2}.

For current densities below 0.3 A cm^{-2} the HRF drops and turns unstable for very low values. For the further characterization of the cell $R_\Omega(i)$ is used since for current densities relevant for the Tafel analysis the deviations between the mean and the specific ohmic resistance are significant.

B.2. Tafel analysis.—After the ohmic resistance has been measured the cell voltage can be reduced by the ohmic losses:

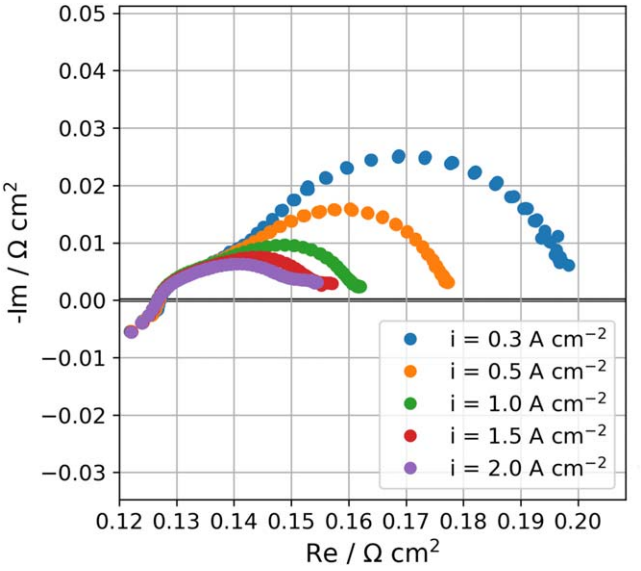

Figure B·1. Nyquist plots for different current densities measured just before CI was performed.

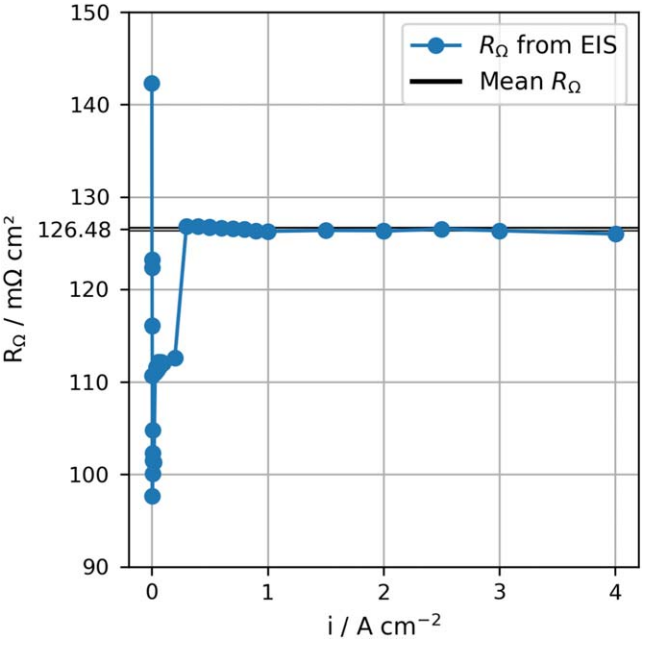

Figure B·2. High frequency resistance measurements for various current densities and mean ohmic resistance.

$$U_{iRfree}(i) = U_{cell}(i) - i \cdot R_\Omega(i) \quad [B\cdot2]$$

The voltage calculated using Eq. B·2 can be reduced by subtracting the Nernst reversible potential U_{rev} from the activation overpotential:

$$\eta_{act}(i) = U_{cell}(i) - i \cdot R_\Omega(i) - U_{rev} \quad [B\cdot3]$$

Equation B·3 is only valid when mass transport losses are insignificant, hence, for small current densities.

The Nernst potential was calculated using the approach from Ref. 36 which is a temperature correction for atmospheric pressure. For the given operating temperature of 80 °C this results in 1.18339 V.

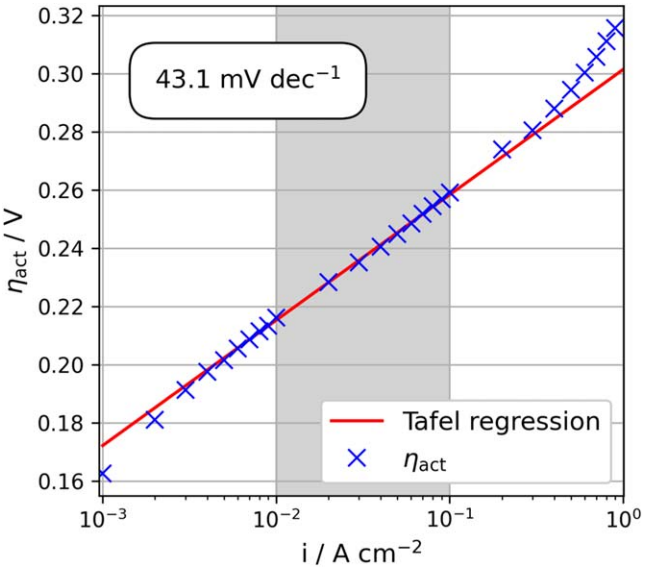

Figure B·3. Tafel plot showing activation overpotential over i: measured activation overpotential and Tafel regression.

$$U_{rev}(T) = 1.5184 - 1.5421 \cdot 10^{-3}\, T + 9.523 \cdot 10^{-5}\, T \cdot \ln(T) + 9.84 \cdot 10^{-8}\, T^2 \quad \text{[B·4]}$$

Figure B·3 shows a Tafel analysis performed for $i \in [0.01\ \text{A cm}^{-2},\ 0.1\ \text{A cm}^{-2}]$ right before the CI experiments were executed.

Mass transport losses can be defined as the residual:

$$\eta_{mt}(i) = U_{cell}(i) - \eta_{act}(i) - \eta_{\Omega}(i) - U_{rev} \quad \text{[B·5]}$$

ORCID

Tobias Krenz https://orcid.org/0000-0001-7170-1945
Torben Gottschalk https://orcid.org/0009-0005-8454-8122
Patrick Trinke https://orcid.org/0000-0002-0935-5321
Boris Bensmann https://orcid.org/0000-0001-8685-7192
Richard Hanke-Rauschenbach https://orcid.org/0000-0002-1958-307X

References

1. D. Bessarabov, H. Wang, H. Li, and N. Zhao, *PEM Electrolysis for Hydrogen Production: Principles and Applications* (CRC Press, Boca Raton) (2016).
2. T. Smolinka, H. Bergmann, J. Garche, and M. Kusnezoff, "The history of water electrolysis from its beginnings to the present." *Electrochemical Power Sources: Fundamentals, Systems, and Applications: Hydrogen Production by Water Electrolysis* (Elsevier, Amsterdam) (2021).
3. A. Godula-Jopek, *Hydrogen Production: By Electrolysis* (John Wiley & Sons, Weinheim) (2015).
4. D. Bessarabov and P. Millet, *PEM Water Electrolysis* (Academic Press, London) Vol. 2 (2018).
5. S. S. Kumar and V. Himabindu, "Hydrogen production by PEM water electrolysis – A review." *Materials Science for Energy Technologies*, **2**, 442 (2019).
6. M. S. Thomassen, A. H. Reksten, A. O. Barnett, T. Khoza, and K. Ayers, *Pem Water electrolysis Electrochemical Power Sources: Fundamentals, Systems, and Applications* (Elsevier, Amsterdam) p. 199 (2022).
7. G. Tsotridis and A. Pilenga, "Development of reference hardware for harmonised testing of PEM single cell fuel cells." *European Comission*, Publications Office of the European Union, Luxembourg (2021), JRC Technical Report.
8. R. O'hayre, S. W. Cha, W. Colella, and F. B. Prinz, *Fuel Cell Fundamentals* (John Wiley & Sons, New Jersey) (2016).
9. P. Sistat and G. Pourcelly, "Chronopotentiometric response of an ion-exchange membrane in the underlimiting current-range. Transport phenomena within the diffusion layers." *Journal of Membrane Science*, **123**, 121 (1997).
10. A. Moya, "Electrochemical impedance of ion-exchange membranes with interfacial charge transfer resistances." *J. Phys. Chem. C*, **120**, 6543 (2016).
11. A. Moya, "Identification of characteristic time constants in the initial dynamic response of electric double layer capacitors from high-frequency electrochemical impedance." *Journal of Power Sources*, **397**, 124 (2018).
12. C. Breitkopf and K. Swider-Lyons, *Springer Handbook of Electrochemical Energy* (Springer, Berlin) (2017).
13. T. Krenz, O. Weiland, P. Trinke, L. Helmers, C. Eckert, B. Bensmann, and R. Hanke-Rauschenbach, "Temperature and Performance Inhomogeneities in PEM Electrolysis Stacks with Industrial Scale Cells." *J. Electrochem. Soc.*, **170**, 044508 (2023).
14. M. E. Orazem and B. Tribollet, *Electrochemical Impedance Spectroscopy* (John Wiley & Sons, New Jersey) (2008).
15. M. Bernt, J. Schröter, M. Möckl, and H. Gasteiger, "Analysis of gas permeation phenomena in a PEM water electrolyzer operated at high pressure and high current density." *J. Electrochem. Soc.*, **167**, 124502 (2020).
16. A. M. Abomazid, N. A. El-Taweel, and H. E. Farag, "Novel Analytical Approach for Parameters Identification of PEM Electrolyzer." *IEEE Transactions on Industrial Informatics*, **18**, 5870 (2021).
17. L. Järvinen, P. Puranen, A. Kosonen, V. Ruuskanen, J. Ahola, P. Kauranen, and M. Hehemann, "Automized parametrization of PEM and alkaline water electrolyzer polarisation curves." *International Journal of Hydrogen Energy*, **47**, 31985 (2022).
18. D. Chen, P. Pei, Y. Li, P. Ren, Y. Meng, X. Song, and Z. Wu, "Proton exchange membrane fuel cell stack consistency: Evaluation methods, influencing factors, membrane electrode assembly parameters and improvement measures." *Energy Conversion and Management*, **261**, 115651 (2022).
19. X. Z. Yuan, C. Song, H. Wang, and J. Zhang, *Electrochemical Impedance Spectroscopy in PEM Fuel Cells: Fundamentals and Applications* (Springer, Berlin) (2010).
20. J. Zhang, *PEM Fuel Cell Electrocatalysts and Catalyst Layers: Fundamentals and Applications* (Springer Science & Business Media, Luxemburg) (2008).
21. M. Rubio, A. Urquia, and S. Dormido, "Diagnosis of PEM fuel cells through current interruption." *Journal of Power Sources*, **171**, 670 (2007).
22. W. Y. Chang, "Application of current switching method to estimate the model parameters of proton exchange membrane fuel cell." *Simulation Modelling Practice and Theory*, **18**, 35 (2010).
23. F. Jaouen and G. Lindbergh, "Transient techniques for investigating mass-transport limitations in gas diffusion electrodes: I. Modeling the cathode." *J. Electrochem. Soc.*, **150**, A1699 (2003).
24. F. Jaouen, G. Lindbergh, and K. Wiezell, "Transient techniques for investigating mass-transport limitations in gas diffusion electrodes: II. Experimental characterization of the PEFC cathode." *J. Electrochem. Soc.*, **150**, A1711 (2003).
25. J. van Der Merwe, K. Uren, G. van Schoor, and D. Bessarabov, "Characterisation tools development for PEM electrolysers." *International Journal of Hydrogen Energy*, **39**, 14212 (2014).
26. C. A. Martinson, G. Van Schoor, K. Uren, and D. Bessarabov, "Characterisation of a PEM electrolyser using the current interrupt method." *International Journal of Hydrogen Energy*, **39**, 20865 (2014).
27. F. N. Büchi, A. Marek, and G. G. Scherer, "In situ membrane resistance measurements in polymer electrolyte fuel cells by fast auxiliary current pulses." *J. Electrochem. Soc.*, **142**, 1895 (1995).
28. T. Mennola, M. Mikkola, M. Noponen, T. Hottinen, and P. Lund, "Measurement of ohmic voltage losses in individual cells of a PEMFC stack." *Journal of Power Sources*, **112**, 261 (2002).
29. B. Burger, *Fraunhofer Institute for Solar Energy Systems Ise* (2017).
30. B. Andreaus and G. Scherer, "Proton-conducting polymer membranes in fuel cells —humidification aspects." *Solid State Ionics*, **168**, 311 (2004).
31. C. Immerz, B. Bensmann, P. Trinke, M. Suermann, and R. Hanke-Rauschenbach, "Understanding electrical under-and overshoots in proton exchange membrane water electrolysis cells." *J. Electrochem. Soc.*, **166**, F1200 (2019).
32. T. Smolinka, E. T. Ojong, and T. Lickert, "Fundamentals of PEM Water Electrolysis." *PEM Electrolysis for Hydrogen Production: Principles and Applications* (CRC Press, Boca Raton) Vol. 11 (2016).
33. A. Weiß, A. Siebel, M. Bernt, T. H. Shen, V. Tileli, and H. Gasteiger, "Impact of intermittent operation on lifetime and performance of a PEM water electrolyzer." *J. Electrochem. Soc.*, **166**, F487 (2019).
34. M. Bernt, A. Hartig-Weiß, M. F. Tovini, H. A. El-Sayed, C. Schramm, J. Schröter, C. Gebauer, and H. A. Gasteiger, "Current challenges in catalyst development for PEM water electrolyzers." *Chemie Ingenieur Technik*, **92**, 31 (2020).
35. P. Millet, "Characterization Tools for Polymer Electrolyte Membrane (pem) Water Electrolyzers." *PEM Electrolysis for Hydrogen Production: Principles and Applications* (CRC Press, Boca Raton) (2016).
36. A. Roy, S. Watson, and D. Infield, "Comparison of electrical energy efficiency of atmospheric and high-pressure electrolysers." *International Journal of Hydrogen Energy*, **31**, 1964 (2006).